INL/JOU-20-58799-Revision-0

UPDATED U3SI2 THERMAL CREEP MODEL AND SENSITIVITY ANALYSIS OF THE U3SI2-SIC ATF

January 2021

Jacob A Yingling, Elwyn Roberts, Travis W. Knight, Austin Freeman, Kyle A Gamble

Changing the World's Energy Future

Idaho National Laboratory

INL is a U.S. Department of Energy National Laboratory operated by Battelle Energy Alliance, LLC

DISCLAIMER

This information was prepared as an account of work sponsored by an agency of the U.S. Government. Neither the U.S. Government nor any agency thereof, nor any of their employees, makes any warranty, expressed or implied, or assumes any legal liability or responsibility for the accuracy, completeness, or usefulness, of any information, apparatus, product, or process disclosed, or represents that its use would not infringe privately owned rights. References herein to any specific commercial product, process, or service by trade name, trade mark, manufacturer, or otherwise, does not necessarily constitute or imply its endorsement, recommendation, or favoring by the U.S. Government or any agency thereof. The views and opinions of authors expressed herein do not necessarily state or reflect those of the U.S. Government or any agency thereof.

INL/JOU-20-58799-Revision-0

UPDATED U3SI2 THERMAL CREEP MODEL AND SENSITIVITY ANALYSIS OF THE U3SI2-SIC ATF

Jacob A Yingling, Elwyn Roberts, Travis W. Knight, Austin Freeman, Kyle A Gamble

January 2021

Idaho National Laboratory
Idaho Falls, Idaho 83415

http://www.inl.gov

Prepared for the
U.S. Department of Energy
Under DOE Idaho Operations Office
Contract DE-AC07-05ID14517

UPDATED U3SI2 THERMAL CREEP MODEL AND SENSITIVITY ANALYSIS OF THE U3SI2-SIC ADVANCED TECHNOLOGY FUEL

J.A Yingling[a*], K.A Gamble[b], Elwyn Roberts[a], R. Austin Freeman[a], and Travis W. Knight[a]
[a]University of South Carolina, Mechanical Engineering Department, Columbia, SC 29208
[b]Idaho National Laboratory, Computational Mechanics and Materials, Idaho Falls, ID 83415

[*]Corresponding Author: Tel. 801 839 4645, Email: jacobay@email.sc.edu
Address: University of South Carolina, 300 Main Street, Columbia, SC 29208

Abstract

U_3Si_2 is a candidate advanced technology fuel (ATF) replacement for UO_2. U_3Si_2's high uranium density and high thermal conductivity are favorable properties in steady-state and accident conditions. Accident performance of this fuel concept is enhanced when paired with a SiC-SiC cladding, due to high oxidation resistance. Performance of this U_3Si_2-SiC concept fuel is compared to that of UO_2-Zr4 fuels by implementing models that describe the properties of U_3Si_2 and SiC-SiC into Idaho National Laboratory's (INL) fuel performance code, BISON. Included in these material models is a thermal creep model for U_3Si_2 based on compressive creep data. The simulated results suggest that the U_3Si_2-SiC concept fuel may serve as a replacement for UO_2-Zr4 fuels during steady-state operation, provided the mSiC layer remains under compression. Through a moderate power history and three 24-month fuel cycles, the mSiC layer remains under compressive stress through a burnup of 80 MWd/kgU. Since failure of the mSiC layer generally occurs prior to significant thermal creep in U_3Si_2, creep is of little importance during fuel-to-cladding contact. A parameter variation study including 3,860 individual simulations with variations in nominal fuel thermal creep rate, cladding thermal conductivity, cladding irradiation creep, cladding gap size, and cladding thickness demonstrated that research priorities for this ATF should revolve around reducing cladding thickness as a means to minimize cladding failure and enhance maximum fuel energy production. Generally, despite advances in SiC-SiC compliance, the brittle nature of mSiC excludes U_3Si_2-SiC for use where fuel cladding contact may occur.

Keywords | multi-physics simulation, nuclear fuel performance, pellet-cladding mechanical interaction, uranium silicide, U3Si2, silicon carbide, SiC, thermal creep

1 Introduction

1.1 Motivation

The goal behind advanced technology fuel (ATF) research is to replace standard light water reactor (LWR) fuel with a fuel that lessens the severity of accidents while maintaining or improving fuel performance [1]. Amongst the candidates for ATFs, uranium silicide (U_3Si_2) is of interest due to its high uranium density and high thermal conductivity. However, due to the limited data available, much of the high burnup in-reactor behavior of U_3Si_2 is not known [2]. Specifically, an experimentally derived model describing the thermal creep of U_3Si_2 is lacking in the literature. This work reports the development of a thermal creep model for U_3Si_2 based on compressive creep experiments performed at the University of South Carolina (UofSC) [3] [4] and demonstrates its effects via finite element simulation.

Replacements for Zircaloy cladding are desired to lengthen the time nuclear operators have to respond to accidents. SiC is under consideration as a cladding material due to its high strength, minimal thermal and irradiation creep, high steam oxidation resistance, and minimal neutron economy penalty [5]. However, due to its brittle nature, monolithic SiC (mSiC) is not suitable for single layer cladding applications and a composite matrix ceramic SiC (SiC-SiC) must be used to allow more gradual failure modes [6]. While the use of SiC-SiC improves the mechanical compliance of a SiC cladding, stresses in the mSiC layer used as an environmental barrier must remain below the threshold for microcracking to avoid the release of fission gases into the coolant [7].

Recent works indicate that SiC claddings require significant development prior to use. He et al. [8] evaluated the failure probability of U_3Si_2 with duplex SiC cladding and found SiC failure to be almost certain under reactivity insertion accident (RIA) conditions. Using BISON, Wei [9] calculated elevated cladding hoop stresses greater than 180 MPa during shutdown which is enough to exceed its

proportional limit stress (PLS) [10]. The resulting microcracking can result in significant fission gas leakage. Rapid failure of SiC cladding is known to occur following pellet cladding mechanical interaction (PCMI) even when cracking compliance of the composite layer is considered [3].

Since the magnitude of U_3Si_2 creep is directly related to cladding stress during contact, accurate prediction of SiC cladding failure in U_3Si_2-SiC simulations requires an improved thermal creep model. Until now, simulations of this concept fuel were completed using Metzger's U_3Si_2 thermal creep model [8], which was developed using Finlay's irradiation and swelling data [11], with kinetic theory [7]. The development of an experimentally derived thermal creep model enhances understanding of the U_3Si_2-SiC fuel system to help identify fuel design priorities.

1.2 Objectives

In this work, the BISON nuclear fuel performance code is used to further understanding of the U_3Si_2 -SiC ATF concept by: (1) developing a full physics simulation for the U_3Si_2-SiC ATF concept, including the experimentally derived thermal creep model developed in this work and the various U_3Si_2 and SiC models of the open literature, (2) providing a predictive simulation comparison of the concept ATF against UO_2-Zr4 fuels, and (3) identifying essential U_3Si_2-SiC ATF design priorities through parameter variation studies to test simulation response to variations in U_3Si_2 thermal creep, SiC thermal conductivity, cladding gap, and SiC-SiC cladding layer thickness.

2 U3Si2 Thermal Creep

2.1 Model data

UofSC thermal creep data [12] is fit using the Mukherjee-Bird-Dorn equation [13]:

$$\dot{\epsilon} = \frac{AGb}{kT}\left(\frac{b}{d}\right)^m \left(\frac{\sigma}{G}\right)^n D_0 e^{-\frac{Q}{RT}} \quad (1)$$

$$\dot{\epsilon} = \frac{A'}{T}\frac{\sigma^n}{d^m} e^{-\frac{Q}{RT}} \quad (2)$$

Equation 1 is an empirical secondary thermal creep model capable of accounting for dislocation and diffusional components through its incorporation of stress, temperature, and grain-size-dependent factors. Due to uncertainties in the original experiment, primary thermal creep of U_3Si_2 was unable to be determined reliably and is excluded from the model [4]. Equation 1 is simplified by collecting leading factors into a single coefficient (A'). When Equation 2 is rearranged, the coefficients A' and Q are found by iterating over values of m and n to calculate a linear least squares fit of $\ln(\dot{\epsilon}\mathrm{T}\mathrm{d}^{\mathrm{m}}\sigma^{-n})$ against T^{-1}.

UofSC received various batches of U_3Si_2 pellets for characterization and creep testing. The data received from INL for determining U_3Si_2 creep coefficients came from compressive creep trials from Batches 3 and 4 [12]. The compressive creep experiment covered a range of temperatures and stresses applicable to LWR conditions. A total of 13 creep tests were conducted on five U_3Si_2 pellets. Tests 1-5 use pellets from Batch 3 for characterization, and Tests 6-13 use pellets from Batch 4. Table 1 below provides the average results of these experiments after applying statistical controls to minimize error when calculating secondary creep for each test [3] [4].

Table 1. Summary of UofSC compressive creep experiments.

Pellet ID	Test #	Creep Rate (1/s)	Average Temperature (K)	Temperature Variation (Std. dev/μ)	Average True Stress (MPa)	Stress Variation (Std. dev/μ)	Time (Hrs)	Grain Size (μm) [14]
150813-A	1	8.7327E-8	1218.37	0.017	44.10	0.034	100	15.6
	2	1.1342E-7	1205.18	0.019	71.77	0.016	100	15.6
	3	N/A	N/A	N/A	N/A	N/A	N/A	N/A
150813-B	4	1.7042E-8	1121.22	0.060	77.66	0.021	433	15.6
	5-A	1.3081E-7	1223.89	0.090	65.13	0.029	105	15.6
	5-B	6.4806E-8	1210.07	0.010	57.71	0.024	200	15.6
161214-B	6	1.5728E-8	1173.59	0.000	46.43	0.009	230	26
	7	4.6342E-8	1223.59	0.000	45.21	0.014	230	26
161214-A	8	1.5486E-8	1223.60	0.000	29.51	0.013	65	26
	9	2.7472E-8	1223.53	0.000	49.73	0.012	135	26
	10	7.1920E-8	1223.64	0.000	63.62	0.006	82	26
161214-C	11	1.1171E-8	1223.69	0.000	26.91	0.020	280	26
	12	1.8750E-8	1273.61	0.000	26.45	0.021	330	26
	13	2.9831E-8	1273.61	0.000	47.79	0.010	140	26

2.2 Model parameters

The average strain rates, temperatures, and true stresses in Table 1 were calculated based on the following requirements: (1) Include a range of data for at least 65 hours of steady-state creep time outside of the first 130 hours to allow sample seating and any primary creep to complete. (2) The experimental average strain rate for this range of data must have a coefficient of correlation (r^2) greater than 0.90. (3) The average temperature and true stress for the range of data must have a coefficient of variation ($\sigma\mu^{-1}$) less than 0.035 to minimize variations in the calculated means.

Table 2. Creep parameters for Equation 2.

A'	n	m	Q (kJ/mol K)
4.841e-19	1.936	1.86	223.1

2.3 Experimental variations

Figure 1 shows the overlap between the measured and calculated strain rates using Equation 2 as a secondary creep model. In Table 2, U_3Si_2 creep coefficients for Equation 2 are found by iterating over values of m between 0 and 5, and of n between 1 and 7 until the highest r^2 is found. The Q and A' creep parameters are found from the slope and intercept of the best fit, respectively. The error bars in Figure 1 are determined by propagating the experimental data variations in temperature and stress through the creep model in Equation 2. In addition to these experimental variations, a 2% systematic variation in the temperature and stress measurements is assumed to account for bias due to measurement technique. Consequently, the combined effect of temperature and stress variations on the calculated creep rate is evident.

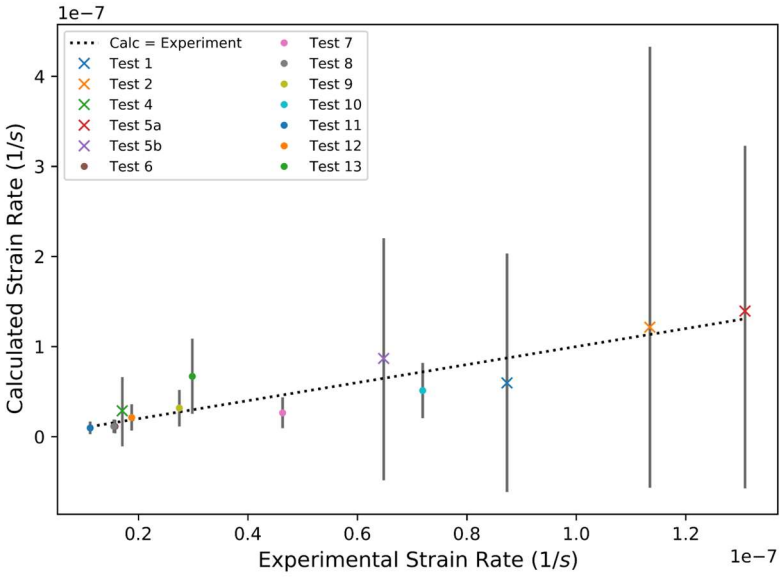

Figure 1. Calculated model vs experimental data (p-value=0.00002, r^2=0.83).

The grain size used in the creep calculations are from Table 1 were determined from pre-creep batch samples using ImageJ software [14]. Experimental variations in grain size were omitted from the error propagation in Figure 1, since the evolution of grain size throughout creep testing is unknown. When the creep parameters of Table 2 are used in Equation 2 and plotted against the experimental values of Table 1, we observe that the data fit to the model within the range of calculated variations.

A notable exception is the calculated strain rate for Test 7, which is unable to match measured experimental values. This discrepancy is explained by the misalignment of Sample 161214-B, which resulted in excessive sample curvature and non-uniform compressive stress during the later stage of the test [4]. Since the experimental strain rate measurement depends on uniaxial stresses, the non-uniform stress condition may have caused heightened stress along a pellet edge, resulting in an erroneously high strain rate measurement. However, considering the overall variations in the experimental data and the generally low thermal creep rate, the errors in Test 7 do not seem large enough to warrant exclusion from the model.

3: BISON Material Models

3.1 Model summary

Finite element analysis methods were used to determine the impact of the developed U_3Si_2 secondary thermal creep model on the performance of the ATF concept. BISON is a finite element analysis code described by others throughout the development of fuel performance models [15] [16]. Table 3 summarizes the material models used in the U_3Si_2-SiC concept ATF BISON simulation. Bold italicized cells represent models either added to the BISON codebase or modified from their original format. Unitalicized cells are material models already available in BISON.

Table 3: Material models used in BISON simulation

	U_3Si_2	Monolithic SiC	Composite SiC
Thermal Expansion	***Obbard*** [17]	Katoh [18]	Katoh [18]
Specific Heat	White [19]	Stone [20]	Koyanagi [21]
Thermal Conductivity	White [19]	Stone [20]	***Koyanagi*** [21] ***modified***
Swelling	Barani [22], Hofmann [23]	Katoh [24]	Katoh [24]
Fission Gas Release	Barani [22]	N/A	N/A
Elasticity	White [19]	***Snead*** [25] ***modified***	***Singh*** [26] ***modified***
Plasticity	N/A	N/A	***Data from Braun*** [27]
Creep	***This work (Thermal)***	***Koyanagi*** [28] [29]	***Koyanagi*** [28] [29]
Fracture/Relocation	***Francher*** [30] ***modified***	N/A	N/A
Densification	None [2]	N/A	N/A

The rod geometry is a duplex SiC cladding that follows the outside monolithic design as suggested by Stone to reduce overall failure probability [20].

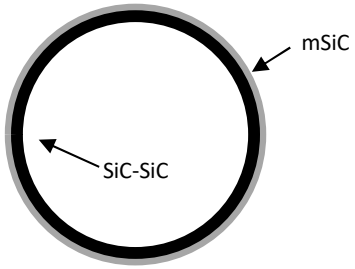

Figure 2: Duplex cladding arrangement.

Stone found that this cladding arrangement ensured compression of the outer mSiC throughout fuel life. By maintaining the outer mSiC in compression, concerns regarding SiC-SiC cracking and loss of hermeticity are lessened. Geometry specifics such as rodlet length and diameter, cladding gap, and cladding layer thicknesses are found in Section 4.1.

3.2 Model development and modification

3.2.1 Thermal expansion of U_3Si_2

Obbard et al. [17] describe the linear coefficient of thermal expansion of U_3Si_2 as Equation 3. Since BISON has existing thermal expansion models in place, Obbard's linear thermal expansion coefficient function was added to the existing code as an option.

$$\alpha(\mathrm{T}) = 2.10 \cdot 10^{-5} - 7.25 \cdot 10^{-9}\mathrm{T} \quad (3)$$

3.2.2 SiC/SiC thermal conductivity

Irradiation damage of SiC is an important part of describing its thermal conductivity. SiC-SiC is modeled by adding Stone's irradiation damage resistivity model to Koyanagi's unirradiated tube specimen thermal diffusivity data in the following manner:

$$k_{nonirr} = \alpha \rho C_p \tag{4}$$

$$R_{nonirr} = k_{nonirr}^{-1} \tag{5}$$

$$R_{irr} = 15.11 \cdot S \tag{6}$$

$$k_{tot} = \frac{1}{R_{irr} + R_{nonirr}} \tag{7}$$

Density (ρ), thermal diffusivity (α), and specific heat (C_p) data for Equation 4 are taken from Koyanagi [21]. Resistivity due to irradiation in Equation 6 is taken from Stone [20]. Non-irradiative thermal resistivity is added to irradiative thermal resistivity in Equation 7 to determine a combined coefficient of thermal conductivity for tubular SiC-SiC.

3.2.3 SiC elasticity

Many of SiC's properties are affected by irradiation damage. This damage is completed prior to 2 dpa of fluence [24]. To account for the irradiation degradation of the elastic modulus, mSiC and SiC/SiC are modeled to linearly degrade the value of the elastic modulus from 460 GPa [25] and 201.9 GPa [31] by 10% and 18.4%, respectively, over 2 dpa [32].

3.2.4 SiC/SiC compliance

Composite matrix ceramic (CMC) materials have an elastic modulus that varies based on a stress-dependent damage coefficient. Braun et al. determined the damage coefficient for SiC-SiC via axial applied stresses [27]. To model this behavior, the elastic modulus for SiC-SiC was damaged proportional to the damage coefficient calculated from Braun's results. The maximum von mises stress from the SiC-SiC cladding is used in this calculation since the damage coefficient was determined for a singly applied axial stress.

3.2.5 SiC irradiation creep

Creep of mSiC and SiC-SiC under irradiation is relatively small and is described by Koyanagi's bend stress ratio (BSR) experiments as having a swelling coupled primary creep region as well as a steady-state secondary creep [28]:

$$\dot{\epsilon}_{\mathrm{tot}} = \dot{\epsilon}_{\mathrm{pri}} + \dot{\epsilon}_{\mathrm{sec}} \tag{8}$$

Primary irradiation creep is coupled to volumetric swelling, $\dot{\epsilon}_{vol}$, through a creep compliance coefficient [26]:

$$\mathrm{K}_{\mathrm{pri}} = \left(3.5626 \cdot 10^{-4}\mathrm{T}^2 - 4.1704 \cdot 10^{-1}\mathrm{T} + 156.8507\right) \mathrm{TPa}^{-1} \tag{9}$$

$$\dot{\epsilon}_{\mathrm{pri}} = \mathrm{K}_{\mathrm{pri}} \sigma \dot{\epsilon}_{\mathrm{vol}} \tag{10}$$

Secondary irradiation creep is proportional to stress and fluence [33], with a compliance coefficient of approximately $\mathrm{K}_{\mathrm{sec}} = 1 \cdot 10^{-7} (\mathrm{MPa\ dpa})^{-1}$ [28]:

$$\dot{\epsilon}_{sec} = K_{sec} \sigma \phi \tag{11}$$

Since the BSR technique only represents SiC creep qualitatively, Koyanagi quantitatively calculated the stress and irradiation damage normalized creep strain for in-reactor CVD SiC tubes [29]. These creep data have shown in-pile creep rates to be between 2 and 17 times higher than BSR estimates. In the parameter variation study in Section 4.4, a scaling factor is introduced to the total creep rate to account for this range of irradiation creep.

3.2.6 Fuel fracture and relocation

U_3Si_2 lacks a developed model to describe its fracture and subsequent relocation during rise to power. However, fuel fracture and relocation are important for accurately describing fuel stress and strain during simulation. A recent post-irradiation examination of U_3Si_2 at INL shows that through 20 MWd/kgU of burnup U_3Si_2 exhibits about 25% of the cracking UO2 would experience under the same conditions [2]. In the absence of a validated cracking model, this work uses the UO_2 ESCORE model already available in BISON, but reduced by a factor of 0.25 as a first approximation. Simulation impact from variations in this factor is studied in the multidimensional parameter variation study hereafter.

3.2.7 Densification and U_3Si_2 thermal conductivity degradation

The material models of the present U_3Si_2-SiC simulation differ from those used by He et al. through the incorporation of the material model improvements indicated in Sections 3.2.1-6 above. Other notable differences include fuel densification and thermal conductivity degradation. He et al. assumes densification is similar to UO_2 [8]. However, since post-irradiation examination indicates that fuel porosity is not impacted at low burnup [2], and that densification is largely a phenomenon evident at low burnups, densification in U_3Si_2 is not considered in this study. Additionally, He et al assumes U_3Si_2 thermal conductivity degrades by 50% over 60 MWd/kgU. Considering the porosity observations given above, this assumption is likely excessive. Since irradiated material properties for U_3Si_2 are sparse in the literature [19], this work makes use of the U_3Si_2 handbook's empirical relation with no thermal conductivity degradation.

4 Results and Discussion

4.1 Simulation conditions

The default models in BISON and those developed above are implemented in simulations to provide a comparative view of the performance differences in three cases: (1) UO_2-Zr4, (2) UO_2-SiC, and (3) U_3Si_2-SiC. The simulation conditions used for this comparison are shown in Table 4 below.

Table 4. Simulation conditions.

Cycle Linear Heat Rate	21.16, 19.3, 17.5 kW/m (three 24-month cycles)
Initial Plenum Pressure	2 MPa
Coolant Pressure	15.31 MPa
Coolant Inlet Temperature	599.95 K
Coolant Flow Rate	3675.4 kg/(m^2-sec)
Rodlet Pitch	12.6 mm
Rodlet Radius	4.75 mm

Fuel-to-Cladding Gap	80 µm
SiC/SiC Thickness	0.6 mm
mSiC Thickness	0.2 mm
Zircaloy Thickness	0.572 mm
Fuel Height (10 pellets)	9.8 cm
Plenum Height	10.38 cm
U_3Si_2 Grain Size	20 µm

Material properties from source code examples provided by BISON were used for UO_2 fuel and Zr4 cladding. External geometry, coolant flow rate, inlet temperature, and pressure in the three simulations are identical.

Since much of the motivation behind using U_3Si_2-SiC is economic, a power history based on a maximum of 40 W/gU was chosen to facilitate 24-month cycles [34]. Relatively small decreases in power were chosen to approximate a fuel shuffling strategy, considering the absence of burnable poisons. Linear heat rates for subsequent cycles are chosen to bring the average burnup of the simulated rodlet to 80MWd/kgU after three cycles.

4.2 Simulation end criteria

Each simulation case was run until one of two possible outcomes occurred: (1) Cladding failure criteria was reached, as discussed below or (2) the target average fuel burnup of 80MWd/kgU was achieved. An average fuel burnup of 80 MWd/kgU was selected as the goal average burnup in this work. Since equally enriched UO_2 fuels are capable of more than 60MWd/kgU, the selection of 80MWd/kgU was a burnup goal based on the higher uranium density of U_3Si_2 [35].

4.2.1 Cladding failure criteria

Cladding failure for U_3Si_2-SiC is defined as reaching a maximum mSiC cladding hoop stress of 173 MPa, the average characteristic failure stress of mSiC determined by Deng [36]. Zr4 cladding failure was taken as an irradiated hoop strain limit, determined by Jernkvist to be 1.3% [37]. These measures of failure are sampled from the entire cladding in the case of Zr4, but only from the monolithic portion of the cladding in the case of SiC.

4.3 Simulation response

4.3.1 Fuel temperature

In Figure 3, maximum, average, and minimum temperatures were calculated to indicate the temperature distribution in the fuel to high burnup. Maximum homologous temperatures (T_{max}/T_m) with melting points of 3138 K and 1938 K for UO_2 and U_3Si_2, respectively, were calculated to indicate the margin to melt within each fuel.

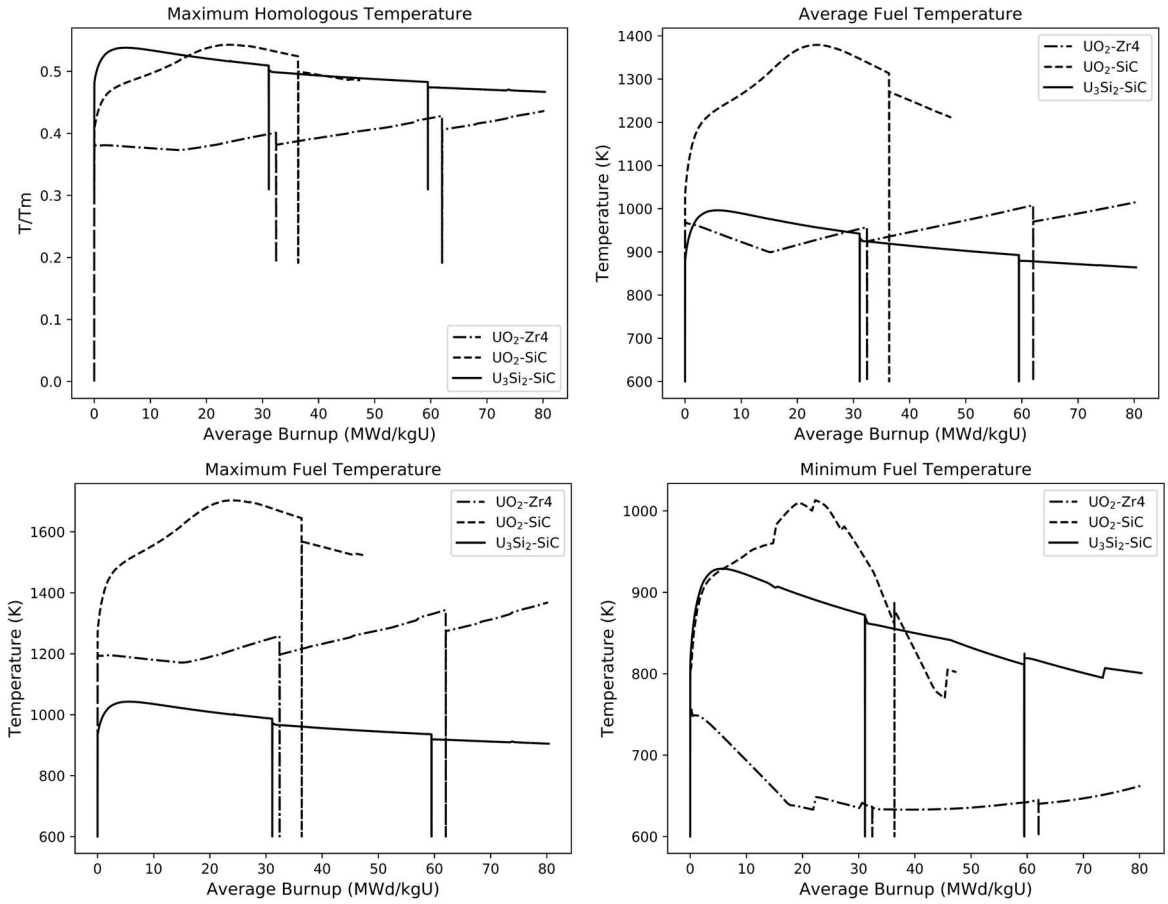

Figure 3. Fuel temperature as a function of average burnup.

Although the U_3Si_2-SiC fuel concept has lower maximum fuel temperatures, it operates at a higher homologous temperature (T/T_m). Irradiative degradation of the SiC cladding is responsible for the large increase in temperature at low burnup. This effect is particularly evident in the case of U_3Si_2-SiC in which the startup T_{max}/T_m increases to above 0.5 during the first 10 MWd/kgU. Though U_3Si_2-SiC generally has a lower steady-state maximum operating temperature, its early T_{max}/T_m is much higher than that of UO_2-Zr4. Unfortunately, T_{max}/T_m remains mostly comparable to UO_2-SiC for much of the simulation.

Performance of UO_2-SiC is substantially worse than the other fuels and only reaches about 50 MWd/kgU before the failure criteria for the SiC cladding has been reached. While the UO_2-SiC simulation ends in the event of cladding failure, U_3Si_2-SiC and UO_2-Zr4 perform identically in this regard as the simulations ran to completion without cladding failure. While U_3Si_2-SiC appears to have some minor benefit at high burnup, in view of the temperature performance shown in Figure 3, it is hard to recommend U_3Si_2-SiC as a replacement for UO_2-Zr4.

The chosen nominal power history is conservative to allow the use of 24-month cycles. However, since the ability to effectively conduct heat at higher temperatures is an advantage of U_3Si_2 fuel, two additional power densities were simulated to explore the extent of U_3Si_2-SiC's acceptable

power limits. Figure 4 below, shows a comparison between the nominal case, 25% and 50% higher power.

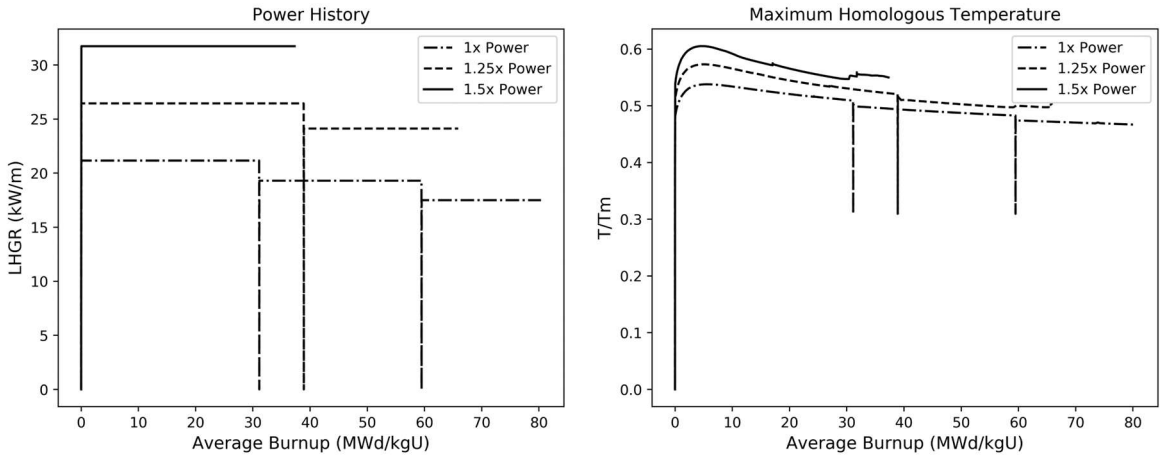

Figure 4. Fraction of melting point in U_3Si_2-SiC for increasingly higher power density.

U_3Si_2's thermal conductivity allows for significant increases in power at the expense of very little decrease in margin to melt. However, despite this advantage, the 25% and 50% power increases both resulted in premature cladding failure at 68 and 38 MWd/kgU, respectively. At typical core power, peak power densities of more than 30 kW/m are common for steady-state lead PWR rods. In light of this, U_3Si_2-SiC cannot be recommended for applications where higher power densities will result in failure of the SiC cladding. These results suggest that limiting LHGR to less that 25 kW/m is necessary to prevent contact and avoid premature cladding failure.

4.3.2 Plenum pressure and fission gas release

There is no validated fission gas release (FGR) model for U_3Si_2; however, the FGR model developed by Barani et al. [22] demonstrates what is generally expected from U_3Si_2 based on rate parameters informed by density functional theory. In Figure 5, the results show no FGR through 80 MWd/kgU. Although, the high-burnup FGR of U_3Si_2 is unknown, the Barani FGR model for U_3Si_2 provides FGR values similar to those established via post-irradiation examination at low burnup [2].

UO_2-SiC FGR is significantly higher than all others due to its excessively large temperature gradient. Considering the added risk of gas leakage due to microcracking in SiC, UO_2 is not recommended when paired with SiC cladding. In this respect, U_3Si_2 has the advantage, primarily due to its higher thermal conductivity that lowers average fuel temperatures at high burnup causing a decrease in the mobility of fission gases. Importantly, the UO_2 fission gas model does not account for high-burnup structures and is not accurate past approximately 50 MWd/kgU. However, even at this moderate burnup, the improved FGR performance of U_3Si_2 is evident.

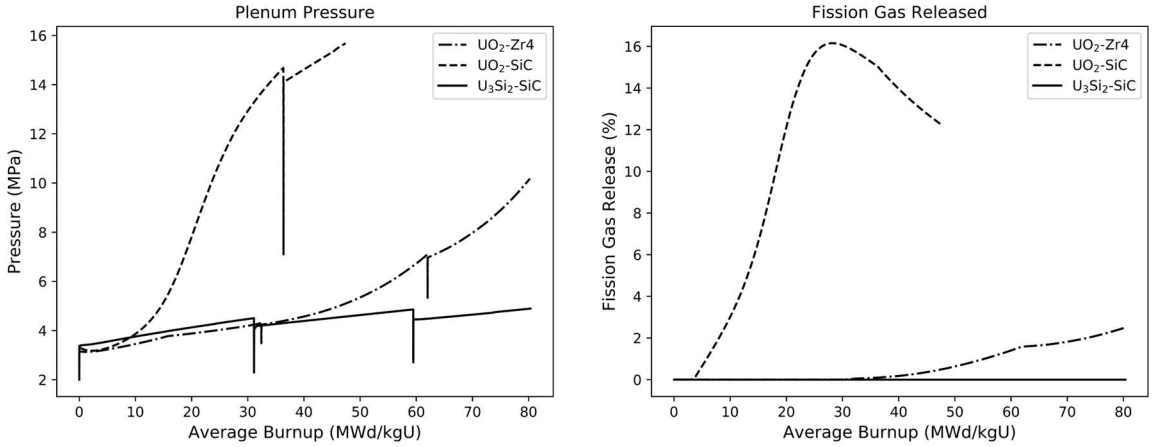

Figure 5. Plenum pressure and fission gas release over average burnup.

The reality of having essentially zero U_3Si_2 FGR is questionable at such high burnups. Such a result can be understood in terms of the model lacking certain physical phenomena, such as increased gas mobility, as a result of microcracking in the fuel or larger driving forces from fission-gas-degraded thermal conductivity. BISON UO_2 material models include these effects, which are partially responsible for its higher FGR. Since high burnup FGR data are unavailable for U_3Si_2, a FGR model coupled to cracking as well as thermal conductivity degradation would be a valuable addition to the simulation of U_3Si_2 performance in BISON.

Despite U_3Si_2 having a much lower FGR, the swelling model developed by Barani shows similarly low swelling. The present simulation indicates that U_3Si_2-SiC is expected to swell approximately half as much as UO_2-Zr4, which is in keeping with expectations set by post-irradiation examination at low burnups. As mentioned previously, the long-term effect of low FGR on fuel swelling in U_3Si_2 needs to be investigated further at higher burnup before such outcomes are to be believed.

4.3.3 Cladding hoop stress

Considering the vast material differences between CMC SiC and Zr4, the distribution of stress through the SiC cladding is expected to be uneven. Figure 6 below indicates the maximum and minimum

hoop stress over burnup for the three fuel combinations.

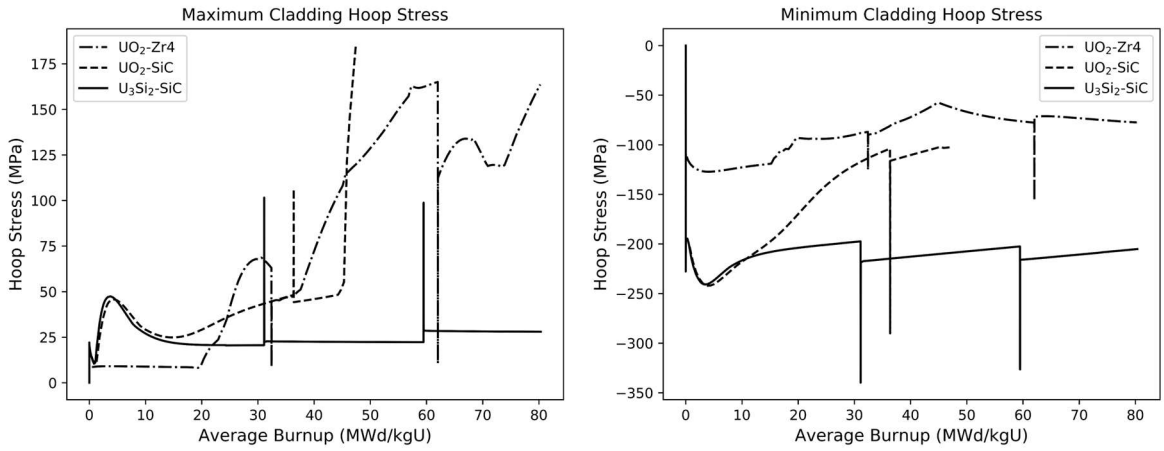

Figure 6. Maximum and minimum cladding hoop stress over average burnup.

For the U_3Si_2-SiC simulation, tensile stresses within the cladding are maintained within the SiC-SiC layer while the mSiC remains under compressive stress. This behavior is desirable since tensile strain of the mSiC layer is a driving factor in microcracking, which has important implications for cladding hermeticity under load. Since the mSiC is maintained under compressive stress, Figure 6 illustrates that tensile stress within the SiC-SiC and mSiC cladding will increase greatly during shutdown. Although the mSiC remains under compressive load, the SiC-SiC layer is placed under tensile stresses exceeding 100 MPa. Considering that a round robin study of tubular CMC SiC properties indicates a PLS of about 92.8 MPa, cracking of the SiC-SiC is expected under normal operating conditions [31].

Figure 6 makes it apparent that combinations of low thermal conductivity fuel and cladding, like UO_2-SiC, provide unacceptable performance under typical LWR conditions. This is especially true when the cladding is susceptible to brittle failure during PCMI. Additionally, although there is some minor fuel temperature benefit from the U_3Si_2-SiC fuel, there is no exceptionally notable performance benefit in terms of cladding performance during normal operation.

4.4 Pellet cladding mechanical interaction

Due to the low power densities and temperatures for U_3Si_2-SiC, no PCMI was found to have occurred during the prior simulation. However, since operational realities like fuel relocation during shuffling and rod inversion between cycles were not included as part of the simulation, insufficient stresses were created to evaluate conditions in which thermal creep of U_3Si_2 may be significant. Under such processes it is conceivable that despite U_3Si_2's relatively lower amount of fuel cracking, fragments of the fuel may relocate to create contact between the fuel and cladding.

To simulate such an occurrence, the relocation of a fragment of fuel into the fuel cladding gap is investigated by choosing an initial cladding gap of 30 microns to force PCMI to occur following the first cycle. In Figure 7 below, the development of maximum and average hoop stress in the cladding are shown.

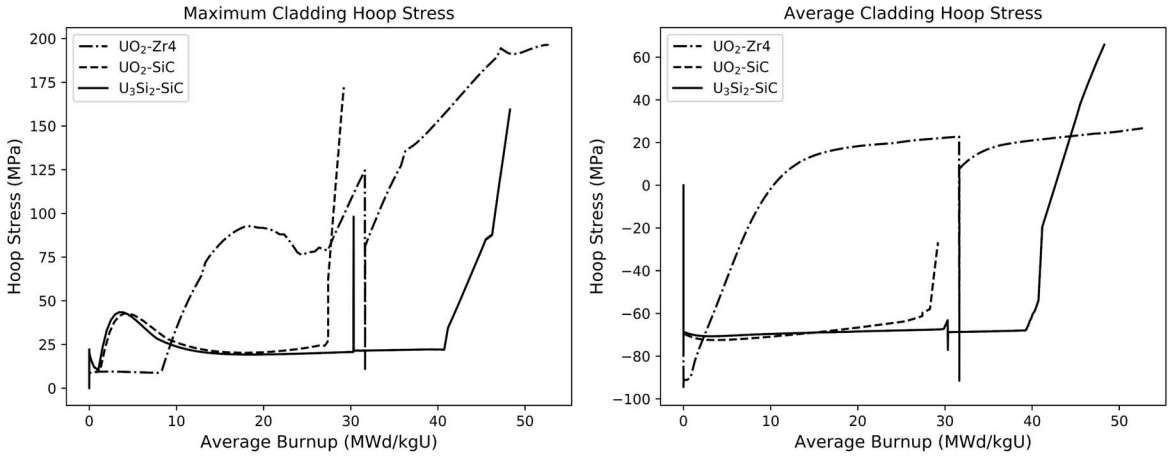

Figure 7. Cladding hoop stress during simulated PCMI using a 30 micron cladding gap.

For U_3Si_2-SiC, rapid development of tensile stress within the cladding is evident during PCMI and causes a stress-based failure of the cladding near 48 MWd/kgU. Increases in both maximum and average hoop stress occur; however, maximum stresses are under a delay. Although contact occurs just before 40 MWd/kgU, a delay of approximately 3 MWd/kgU follows before maximum hoop stress begins to increase. This is in part due to the cracking compliance of the SiC-SiC layer evident in the decreasing slope of the average hoop stress in Figure 7 near 40 MWd/kgU. The delay between contact and cladding failure is significant, which indicates that material design efforts to improve SiC-SiC compliance have an important role in preventing SiC cladding failure.

Of particular importance is the difference in cladding failure among UO_2-Zr4, UO_2-SiC, and U_3Si_2-SiC. PCMI for UO_2-Zr4 occurs through more than 40 MWd/kgU before failure; whereas, for U_3Si_2-SiC the cladding survives for less than 10 MWd/kgU. UO_2-SiC is the least compliant and the cladding fails within 4 MWd/kgU of contact. Regardless of the creep differences between UO_2 and U_3Si_2, the brittleness of SiC results in rapid failure of the cladding following PCMI for both UO_2-SiC and U_3Si_2-SiC.

In addition to using the 30 micron cladding gap, additional simulation cases were run for U_3Si_2-SiC using 0.1x, 1x, and 10x the nominal thermal creep rate for the model determined in Section 2. Nearly identical hoop stresses were obtained in each case, indicating that thermal creep of U_3Si_2 has little impact on mitigating cladding failure during PCMI. Given the low temperature in the fuel, thermal and irradiation creep of U_3Si_2 are low regardless of stress in the current model. Considering the BISON UO_2 thermal creep model is well understood, the rapid failure of SiC for both UO_2 and U_3Si_2 suggests that it is unlikely that creep of the fuel is capable of compensating for the brittle nature of SiC. Even with improved SiC-SiC layer compliance, stresses in the mSiC layer result in rapid failure of the cladding.

The reader is advised that the thermal creep model for U_3Si_2 was developed using compressive creep data between 25 and 78 MPa. As such, no experimental data were available to inform the development of the U_3Si_2 thermal creep model at fuel stresses that are typical during PCMI. Because of this, the creep behavior of U_3Si_2 at very high stresses is unknown and the PCMI behavior of U_3Si_2-SiC in Figure 7 is an extrapolation subject to skepticism. Be that as it may, in light of the similarly rapid failure of UO_2-SiC for which creep is well understood, the PCMI behavior of U_3Si_2-SiC appears to be reasonable.

As discussed in Section 2.1, primary creep of U_3Si_2 is not included in the U_3Si_2 thermal creep model. Since primary creep would have a significant influence during the high stresses that occur during PCMI, there is substantial need for future experimental work to explore thermal creep of U_3Si_2 for stresses exceeding 100 MPa. Since U_3Si_2 has many metal-like properties, it may be that such a study would uncover significant creep during pellet cladding contact and improve the viability of SiC as a nuclear fuel cladding.

4.5 Multidimensional parameter study

4.5.1 Design parameter variations

The nominal parameter values used in the above analysis demonstrate the expected performance differences among UO_2-Zr4, UO_2-SiC, and U_3Si_2-SiC. However, despite the efforts involved in establishing the nominal case, it is expected that variations caused by uncertainties will exist in these parameters. Due to assumptions made while developing models for U_3Si_2 relocation, cracking, U_3Si_2 thermal creep, SiC monolithic and composite irradiation creep, and thermal conductivity, a variation study on these parameters was completed in combination with design variations in rod geometry due to cladding gap and composite thickness.

Exactly 3860 individual simulations were calculated to develop an understanding of the main effects that each parameter variation has on the simulation responses of maximum fuel temperature, cladding stress, cladding strain, and plenum pressure. The resulting plots of main effects demonstrate the average maximum value of each response with respect to every possible combination of parameter variations. This strategy allows succinct display of the mean maximum response value expected for any specified system parameter. As an indication of how much other parameter variations influence the response, error bars are displayed for one standard deviation above and below the average maximum calculated response.

Variations in composite thickness, gap thickness, composite SiC thermal conductivity, fuel creep, and transient SiC irradiation creep are the parameter variations investigated in this study. The mSiC is maintained at a constant 0.2 mm as an environmental barrier layer to ensure complete hermeticity of the entire cladding package despite SiC-SiC cracking. Since lab scale SiC-SiC claddings have been produced with thicknesses as low as 350 microns [6], it is assumed that production of reliable SiC-SiC is possible at a thickness of 450 microns. Rod diameter is fixed in this parameter variation study so varying SiC-SiC thickness and cladding gap cause the pellet diameter to change accordingly.

The range in fuel creep scaling is somewhat arbitrary. However, due to the compressive nature of the experimental creep testing being opposite to the tensile creep found in LWR fuels, a factor of 10 is likely enough to capture this difference. A 24% variation in SiC-SiC thermal conductivity represents uncertainties from experimental error and unexpected irradiation damage to the cladding. SiC-SiC transient irradiation creep is varied by a factor of up to 17 to account for the range of differences between BSR measurements and those found in-pile [28] [29].

In addition to the parameter variations discussed above, cases were run to test variations in fuel relocation and monolithic thermal conductivity. These were found to have a negligible impact on every response of interest and are omitted from the figures for the sake of brevity.

4.5.2 Fuel temperature and monolithic SiC stress

As expected, Figure 8 demonstrates that variations in SiC-SiC thermal conductivity, cladding gap, and SiC-SiC thickness have predictable effects on maximum fuel temperature. In other words,

phenomena that improve thermal conductivity result in a lower mean maximum fuel temperature. In Figure 8, the average maximum fuel temperature among 3860 simulations show that very large changes in cladding thickness and cladding gap are possible with small changes to fuel temperature. However, the utility of main effects diagrams is found in selecting a design parameter that produces a specified system response to determine the constraints upon other design parameters.

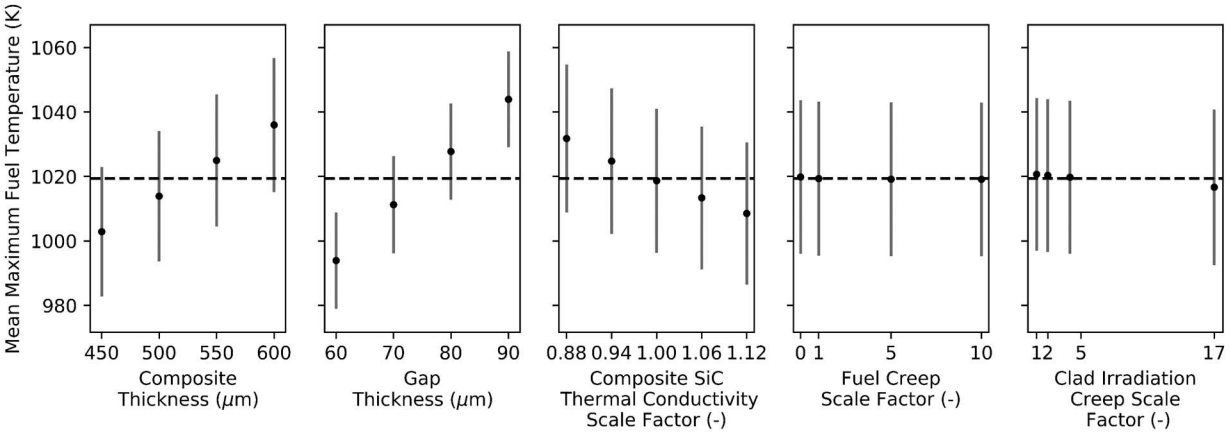

Figure 8. Maximum fuel temperature response to variations in design parameters.

For example, according to Figure 8, if one desires a maximum fuel temperature of around 1000 K, a cladding gap of 60 microns might be chosen as a design parameter to achieve that goal. In Figure 9, however, for a 60 micron cladding gap, there is significant variation in the mean maximum hoop stress in the monolithic cladding indicating that severe compromises in other design parameters would be necessary to maintain stress within the mSiC at an acceptable level. On the other hand, for a gap of 70 microns this variation in hoop stress is nearly eliminated which allows for more flexibility in choosing other design parameters. Further, a 70 micron gap thickness requires little compromise in fuel temperature.

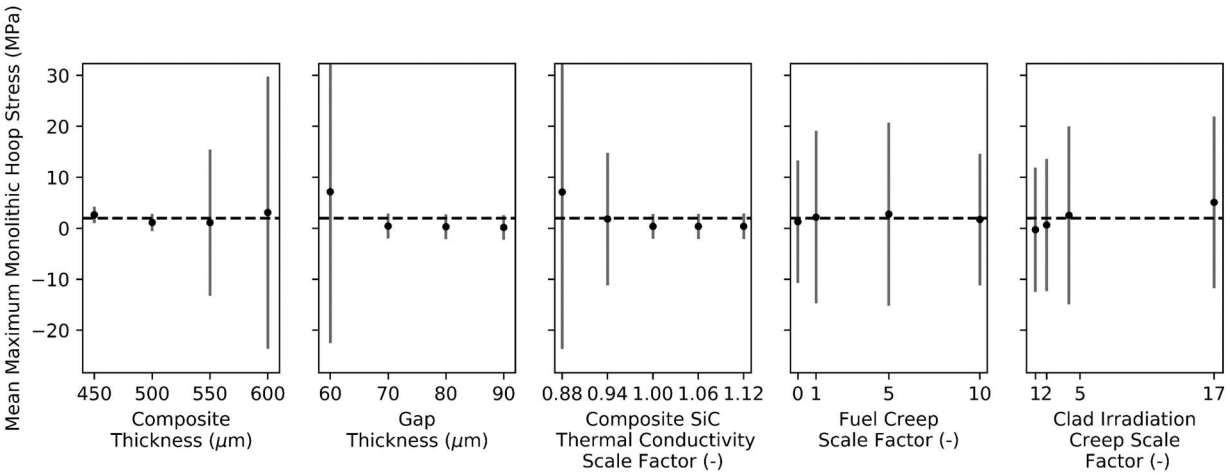

Figure 9. Maximum mSiC hoop stress response to variations in design parameters.

Considering variations in mSiC hoop stress, generally a SiC-SiC thickness of less than 500 microns and cladding gaps of greater than 70 microns are recommended. Thermal conductivity variations have a minor effect on fuel temperature. Despite this, SiC-SiC conductivity should not be allowed to degrade below the nominal case as hoop stress variations become significantly larger and additional compromises to other design parameters would be required to achieve adequately low stress within the mSiC cladding. In the ranges investigated in this study, fuel thermal creep and cladding irradiation creep are negligible factors in terms of response variation and performance on mSiC hoop stress and fuel temperature. Indeed, with the exception of composite stress discussed below, thermal and irradiation creep was, on average, of minor influence on the various tested system responses.

4.5.3 Composite stress

In the literature, irradiation creep in SiC simulations has been considered small. This study applied a linear scale factor to the transient portion of SiC-SiC irradiation creep and found that, except for SiC-SiC hoop stress within the composite layer, irradiation creep is of little importance. Previous work indicates that irradiation creep will have a small deleterious effect on cladding stresses during PCMI [3]; however, for cases where the majority of simulations reach design burnup, the effect of irradiation creep can be ignored.

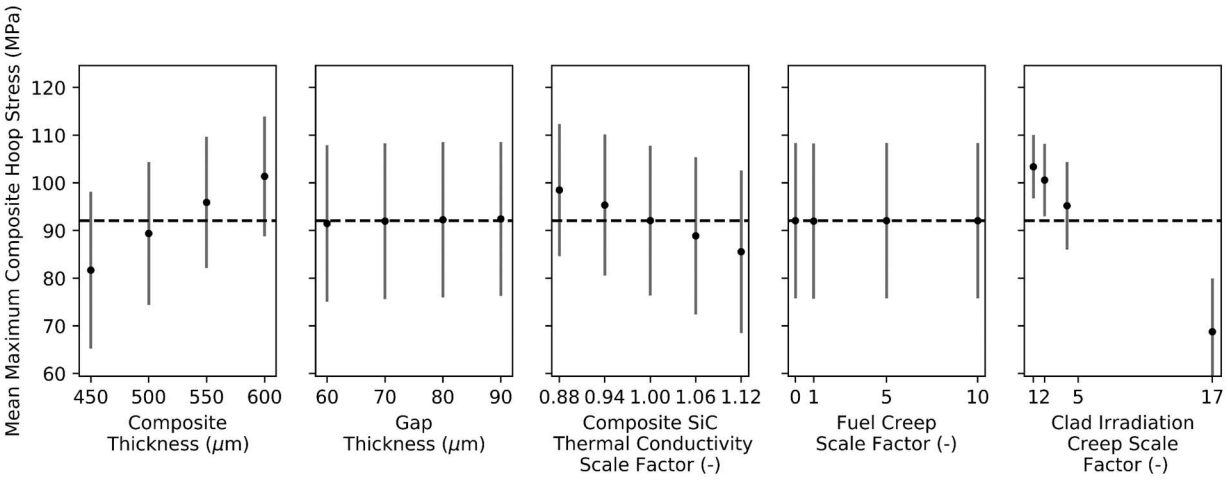

Figure 10. Average of maximum SiC-SiC hoop stress response to variations in design parameters.

Apart from thin composite layers with wide cladding gaps there are, on average, no parameter combinations that prevent hoop stresses that will exceed the SiC-SiC PLS and induce cracking. This is especially true in the near-nominal irradiation creep cases.

5 Conclusion

For stresses between 25 and 78 MPa, and U_3Si_2 pellets fabricated by INL circa 2016, thermal creep follows the Mukherjee-Bird-Dorn relationship of Equation 2 along with the creep parameters of Table 2. U_3Si_2 thermal creep was calculated to be very small during nominal simulation conditions, even in the 10x nominal case. In the nominal simulation, pellet clad contact was completely avoided through an average burnup of 80MWd/kgU indicating that SiC cladding would be mechanically viable for use with high thermal conductivity fuels during normal operating conditions and low power density. Performance of U_3Si_2-SiC at high power density and during PCMI is very poor. UO_2-SiC underperformed

in every metric, emphasizing the importance of avoiding combinations of SiC with low thermal conductivity fuels.

Since U_3Si_2 operates at very low temperatures, it shows little sensitivity to design parameters except fuel to cladding gap and SiC-SiC layer thickness. Fuel creep has little influence on reducing the cladding stress due to PCMI. Thus, because the SiC cladding has no appreciable ductility, premature PCMI failures can readily occur if the fuel comes in contact with the cladding. Hence, fragment relocation during fuel shuffling, or dislodged pellet chips introduced during manufacture are of particular concern to this fuel concept.

Considering these outcomes, a composite layer thickness of less than 500 microns and a cladding gap of greater than 70 microns is recommended in U_3Si_2-SiC fuel designs. Strategies to minimize composite layer thickness without compromising monolithic layer hermeticity are of greatest interest to this concept fuel as they have the largest impact on heat transfer and can prevent fuel cladding contact. Further studies are needed to verify thermal creep of U_3Si_2 under high stress conditions. Without any contrary evidence, U_3Si_2 creep compliance is insufficient to accommodate the brittle nature of SiC during PCMI. Thus, U_3Si_2-SiC cannot be recommended for use cases where fuel cladding contact may occur.

Data Availability

The compressive creep data necessary to reproduce the U_3Si_2 creep model are available at the following url: https://data.mendeley.com/datasets/5p66twxgtg/1

This research was performed using funding received from the DOE Office of Nuclear Energy's Nuclear Energy University Programs; and the Nuclear Regulatory Commission fellowship program. The manuscript has been authored by a contractor of the U.S. Government under Contract DE-AC07-05ID14517. Accordingly, the U.S. Government retains a non-exclusive, royalty free license to publish or reproduce the published form of this contribution, or allow others to do so, for U.S. Government purposes.

References

[1] J. J. Powers, "Early Implementation of SiC cladding fuel performance models in BISON," Oak Ridge National Laboratory, Oak Ridge, 2015.

[2] F. Cappia and J. M. Harp, "Postirradiation examinations of low burnup U3Si2 fuel for light water reactor applications," *Journal of Nuclear Materials,* pp. 62-79, 2019.

[3] J. A. Yingling, "Bison Simulation-Based Identification of Important Design Criteria for U3SI2 Fuels With Composite-Monolithic Duplex SiC Cladding," Scholar Commons, Columbia, 2019.

[4] E. A. C. Mercado, "High Temperature Compression Creep of U3Si2," University of South Carolina, Columbia, 2018.

[5] A. Oizumi, H. Akie, N. Iwamoto and T. Kugo, "Evaluation of neutron economical effect of new cladding materials in light water reactors," *Journal of Nuclear Science and Technology,* vol. 51, pp. 77-90, 2014.

[6] J. D. Stempien, D. M. Carpenter, G. Kohse and M. Kazimi, "Characteristics of Composite Silicon Carbide Fuel Cladding after Irradiation under Simulated PWR Conditions," *Nuclear Technology,* vol. 183, no. 1, pp. 13-29, 2013.

[7] K. E. Metzger, "Analysis of Pellet Cladding Interaction and Creep of U3Si2 Fuel for Use in Light Water Reactors," University Of South Carolina, Columbia, 2016.

[8] Y. He, K. Shirvan, Y. Wu and G. H. Su, "Fuel performance optimization of U3Si2-SiC design during normal, power ramp and RIA conditions," *Nuclear Engineering and Design,* vol. 353, p. 110276, 2019.

[9] L. Wei and S. Koroush, "U3Si2-SiC fuel performance analysis in BISON during normal operation," *Annals of Nuclear Energy,* vol. 132, pp. 34-45, 2019.

[10] C. H. Bumgardner, F. M. Heim, D. C. Roache, A. Jarma, P. Xu, R. Lu, E. Lahoda, B. P. Croom, C. P. Deck and X. Li, "Unveiling hermetic failure of ceramic tubes by digital image correlation and acoustic emission," *Journal of the American Ceramic Society,* pp. 1-14, 2019.

[11] M. R. Finlay, G. L. Hofman and J. L. Snelgrove, "Irradiation Behavior of Uranium Silicide Compounds," *Journal of Nuclear Materials,* vol. 325, no. 2-3, pp. 118-128, 2004.

[12] T. W. Knight, "U3Si2 Fabrication and Testing for Implementation into the BISON Fuel Performance Code," DOI: 10.2172/1434631, 2018.

[13] M. A. Meyers and K. K. Chawla, Mechanical Behavior of Materials, Cambridge: Cambridge University Press, 2009.

[14] C. F. Terrapin, "Unpublished Work," 2018.

[15] K. A. Gamble, A. F. Williams and P. K. Chan, "A Three-dimensional Analysis of the Local Stresses and Strains at the Pellet Ridges in a Horizontal Nuclear Fuel Element," in *Proceedings of the 22nd International Conference on Nuclear Engineering*, 2014.

[16] J. D. Hales, R. L. Williamson, S. R. Navascone , D. M. Perez, B. W. Spencer and G. Pastore, "Multidimensional multiphysics simulation of TRISO particle fuel," *Journal of Nuclear Materials,* vol. 443, no. 1-3, pp. 531-543, 2013.

[17] E. G. Obbard, K. D. Johnson, P. A. Burr, D. A. Lopes, D. J. Gregg, K. D. Liss, G. Griffiths, N. Scales and S. C. Middleburgh, "Anisotropy in the Thermal Expansion of Uranium Silicide Measured by Neutron Diffraction," *Journal of Nuclear Materials,* vol. 508, pp. 516-520, 2018.

[18] Y. Katoh, K. Ozawa, C. Shih, T. Nozawa, R. J. Shinavski, A. Hasegawa and L. L. Snead, "Continuous SiC Fiber, CVI SiC Matrix Composites for Nuclear Applications: Properties and Irradiation Effects," *Journal of Nuclear Materials,* vol. 488, pp. 448-476, 2014.

[19] J. T. White, "Update to the U3Si2 Property Handbook," Los Alamos National Laboratory, Los Alamos, 2018.

[20] J. G. Stone, R. Schleicher, C. P. Deck, G. M. Jacobsen, H. E. Khalifa and C. A. Back, "Stress Analysis and Probabilistic Assessment of Multi-Layer SiC-Based Accident Tolerant Nuclear Fuel Cladding," *Journal of Nuclear Materials,* vol. 466, pp. 682-697, 2015.

[21] T. Koyanagi, Y. Katoh, G. Jacobsen and C. Deck, "Handbook of LWR SiC/SiC Cladding Properties - Rev 1," Oak Ridge National Laboratory, 2018.

[22] T. Barani, G. Pastore, D. Pizzocri, C. Matthews, A. Alfonsi, K. A. Gamble, P. V. Uffelen, L. Luzzi and J. D. Hales, "Multiscale modeling of fission gas behavior in U3Si2 under LWR conditions".

[23] G. L. Hofman, "Crystal Structure Stability and Fission Gas Swelling in Intermetallic Uranium Compoints," *Journal of Nuclear Materials,* vol. 140, no. 3, pp. 256-263, 1986.

[24] Y. Katoh, T. Koyanagi, J. L. McDuffee, L. L. Snead and K. Yueh, "Dimensional Stability and Anisotropy of SiC and SiC-Based composites in Transition Swelling Regime," *Journal of Nuclear Materials,* vol. 499, pp. 471-479, 2018.

[25] L. L. Snead, T. Nozawa, Y. Katoh, T. S. Byun, S. Kondo and D. A. Petti, "Handbook of SiC Properties for Fuel Performance Modeling," *Journal of Nuclear Materials,* vol. 371, pp. 329-377, 2007.

[26] G. Singh, K. Terrani and Y. Katoh, "Thermo-mechanical assessment of full SiC/SiC composite cladding for LWR applications with sensitivity analysis," *Journal of Nuclear Materials,* vol. 499, pp. 26-143, 2018.

[27] J. Braun, C. Sauder, J. Lamon and F. Balbaud-Célérier, "Influence of an original manufacturing process on the properties and microstructure of SiC/SiC tubular composites," *Composites Part A 123,* pp. 170-179, 2019.

[28] T. Koyanagi, Y. Katoh, K. Ozawa, K. Shimoda, T. Hinoki and L. L. Snead, "Neutron-irradiation creep of silicon carbide materials beyond the initial transient," *Journal of Nuclear Materials 478,* pp. 97-111, 2016.

[29] T. Koyanagi, K. Terrani, T. Karlsen, V. Andersson, D. Sprouster, L. Ecker and Y. Katoh, "In-pile tensile creep of chemical vapor deposited silicon carbide at 300C," *Journal of Nuclear Materials 521,* pp. 63-70, 2019.

[30] R. B. Fancher, I. B. Fiero, H. Freeburn, A. M. Garde, M. W. Kennard, M. A. Krammen, P. G. Smerd and N. T. Yackle, "ESCORE: the EPRI Steady-State Core Reload Evaluator Code," Oak Ridge National Laboratory, Oak Ridge, 1987.

[31] G. Singh, S. Gonczy, C. Deck and E. Lara-Curzio, "Interlaboratory round robin study on axial tensile properties of SiC-SiC CMC tubular test specimens," *International Journal of Applied Ceramic Technology,* pp. 1334-1349, 2018.

[32] G. Singh, T. Koyanagi, C. Petrie, C. Deck, K. Terrani, J. D. Arregui-Mena and Y. Katoh, "Elastic moduli reduction in SiC-SiC tubular specimen after high heat flux neutron irradiation measured by resonant ultrasound spectroscopy," *Journal of Nuclear Materials,* vol. 523, pp. 391-401, 2019.

[33] C. A. Lewinsohn, M. L. Hamilton, G. E. Youngblood, R. H. Jones, F. A. Garner, S. L. Hecht and A. Kohyama, "Irradiation-enhanced creep in SiC: data summary and planned experiments," *Journal of Nuclear Materials,* pp. 36-46, 1998.

[34] C. Hove, "24-month PWR fuel cycles - Two decades of AREVA design and operating experience," 2015.

[35] Nuclear Energy Agency, Very High Burn-ups in Light Water Reactors, OECD , 2006.

[36] Y. Deng, S. Koroush, W. Yingwei and S. Guanghui , "Probabilistic view of SiC/SiC composite cladding failure based on full core thermo-mechanical response," *Journal of Nuclear Materials,* vol. 507, pp. 24-37, 2018.

[37] L. O. Jernkvist, "Prediction of Failure of Highly Irradiated Zircaloy Clad Tubes under Reactivity Initiated Accidents," in *Transactions of the 17th Internation Conference on Structural Mechanis in Reactor Technology*, Prague, 2003.

[38] A. Mohamad, Y. Ohishi, H. Muta, K. Kurosaki and S. Yamanaka, "Thermal and mechanical properties of polycrystalline U3Si2 synthesized by spark plasma sintering," *Journal of Suclear Science and Technology 55,* pp. 1141-1150, 2018.